Magnesium Technology 2011
Edited by: Wim H. Sillekens, Sean R. Agnew, Neale R. Neelameggham, and Suveen N. Mathaudhu
TMS (The Minerals, Metals & Materials Society), 2011

HOT WORKABILITY OF ALLOY WE43 EXAMINED USING HOT TORSION TESTING

F. John Polesak III[1], Bruce Davis[2], Rick DeLorme[2], Sean R. Agnew[1]

[1]Department of Materials Science and Engineering, University of Virginia, Charlottesville, Virginia, USA 22904-4745
[2]Magnesium Elektron North America, Madison, Illinois, USA 62060

Keywords: WE43, hot torsion, dynamic strain aging, dynamic recrystallization, homogenization

Abstract

While rare earth additions can impart a variety of property improvements in magnesium alloys, they can also limit the processing parameter window inside which the alloys may be successfully wrought in commercial production routes such as extrusion and rolling. In the present work, hot torsion testing is used to explore the temperature and rate sensitivity of the flow stress of the alloy WE43 in order to establish the boundaries of this processing window. Two mechanisms appear to be important from a fundamental perspective: first, dynamic recrystallization appears to be a prerequisite for significant plastic flow; second, serrated flow and negative strain rate sensitivity are observed at lower deformation temperatures (T ≈ 150-250°C). The Sellars-Tegart model and simple power law, both of which have been successfully applied to describe the temperature/strain-rate/flow stress relationship in AZ31 and many other Mg alloys, are explored in the context of WE43.

Introduction

Magnesium is of interest for myriad applications due to its low density and high specific strength, as compared to competing materials such as aluminum, steel, and polymers. One of the main areas that traditional magnesium alloys lack is high temperature (above 100°C) strength [1]. Magnesium alloy WE43, which contains magnesium, yttrium, neodymium, zirconium, and other rare earth elements, retains its strength at temperatures up to 300°C, and remains stable for long term exposure up to 250°C [2]. In addition, WE43 has good corrosion and ignition resistance [2, 3].

The objective of the current study is to determine the deformation processing conditions (temperature and strain rate) for alloy WE43. Hot torsion testing data were used to compare the flow behavior of samples with different heat treatments. WE43 was examined in the as-cast and vendor-prescribed solutionized conditions. Optical microscopy, scanning electron microscopy (SEM), and energy dispersive spectroscopy (EDS) were employed to qualitatively compare the microstructure and composition of WE43 in the different conditions. Previous studies have reported a wide variety of microstructures at different conditions (as-cast and several heat treatments) including various second phases such as a grain boundary eutectic, Mg-RE precipitates, nanoscale cuboids, and zirconium-rich particles [4, 5, 6, 7, 8]. The presence of these and others phases and their effect on the mechanical behavior was investigated.

The flow behavior of magnesium alloys is often described by a conventional power relation, the Sellars-Tegart equation, or similar equations involving the strain-rate, temperature, and activation energy [7, 8, 9, 10, 11, 12, 13]. It will be shown that a power law can describe the relationship between the flow stress and the Zener-Holloman parameter (i.e. the temperature-compensated strain rate) in the high temperature (T ≥ 350°C) regime.

Experimental Procedures

Hot torsion tests were carried out on a custom Instron torsion machine at equivalent strain rates of 10^{-3}, 10^{-2}, 0.1, 1.0, and 5.0 s^{-1}. The motivation for torsion testing is that the samples do not undergo significant shape change during tests to high strains. Localizations such as necking and barreling that occur during tension and compression, respectively, are avoided in torsion, making it an appealing method of deformation. Another attractive feature of torsion is that a constant true strain rate is imposed by twisting one end of the sample at a constant angular velocity relative to the other end [14]. The solid cylindrical test specimens were machined on a lathe, and had a gage length of 22.225 mm, and a radius of 3.175 mm (Fig. 1). All strains and strain rates reported in this paper are the values at the surface of the gage region. Tests were performed at temperatures of 150, 250, 350, 375, 400, 425, and 450°C. An infrared furnace was used to heat the samples and hold them at temperature for 10 minutes prior to testing. At the higher rates of 0.1, 1.0 and 5.0 s^{-1}, the effect of adiabatic heating was taken into account and calculated to obtain an estimate of the actual testing temperature, which affects the subsequent analyses.

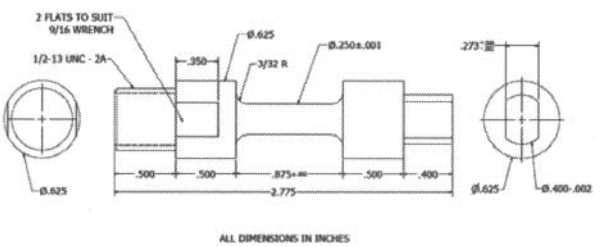

Figure 1. Torsion sample geometry and dimensions, courtesy of Professor J.J. Jonas, McGill University, Montreal, QC, Canada.

The effective stress and strain were calculated according to the von Mises yield criterion from the acquired torque-twist data using the following relationships:

$$\sigma = (\sqrt{3}\,M)/(2\pi r^3)\,(3 + m + n) \quad (1)$$

$$\varepsilon = 2\pi N r/(\sqrt{3}\,l) \quad (2)$$

where M is the measured torque, r is the sample radius, N is the number of revolutions, l is the gage length of the sample, m is the strain-rate sensitivity coefficient at constant strain, and n is the strain hardening coefficient at constant strain rate [12, 14, 15]. The value of m can obtained from log-torque-log-twist rate plots, and in this paper is initially taken to be 0.132 from Gao et al. [15]. The value of n can be obtained from log-log torque-twist plots, but is initially taken as zero in this study, as is commonly done for hot torsion testing [14].

Some readers may question the use of the von Mises isotropic flow rule, but, as detailed below, the material is tested in a randomly textured, i.e. initially isotropic condition. A deformation texture could obviously develop during the tests. However, as shown by Ball and Prangnell for related alloy, WE54, the texture is expected to evolve rather slowly relative to other Mg alloys during hot deformation [16]. Further, Jain and Agnew showed that twinning-induced strength asymmetry diminishes at about 200°C, even in relatively strongly textured alloy AZ31 [17].

The torsion samples were received in the as-cast condition. Torsion specimens and metallographic samples were solutionized at 525°C for 8 hours, followed by a hot water quench. The metallographic samples were then cold-mounted for optical and scanning electron microscopy. Standard metallographic grinding and polishing was performed with SiC grinding paper and an oil-based diamond suspension, respectively. After polishing to ¼-μm, samples were polished with 0.02-μm colloidal silica. Care was taken after each step to fully cleanse the sample with ethanol. Select samples were etched with an acetal-nitric and/or an acetal-picric solution for optical microscopy.

SEM and EDS were performed on a JEOL 840 with a LaB_6 filament. EDS was performed on the polished samples at an accelerating voltage of 15.0 kV, a working distance of 15mm and a probe current necessary to keep the dead time at ~30%. Different areas of the material were analyzed using EDS, including the bulk matrix, grain boundaries, and second phases. The nominal composition of alloy WE43B is shown in Table I, along with the characteristic x-ray energies of interest. It can be seen that some of the M_α energies of the rare earth elements are very close to the K_α energy of magnesium. Because of this, only a qualitative comparison of the various spectra was used to assess compositional variation throughout the samples.

Table I. Nominal composition of WE43B and the corresponding characteristic x-ray energies (keV) [2].

	wt%	K_α	L_α	M_α
Yttrium	3.7-4.3	14.933	1.922	-
Neodymium	2.0-2.5	37.185	5.230	0.978
Ytterbium	0-2.4	52.035	7.414	1.521
Erbium	0-2.4	48.818	6.948	1.406
Dysprosium	0-2.4	45.728	6.495	1.293
Gadolinium	0-2.4	42.761	6.059	1.185
Zirconium	0.4 min	15.746	2.042	-
Magnesium	Balance	1.254	-	-

Results and Discussion

Comparison of as-cast and homogenized microstructure

Scanning electron and optical microscopy of the as-cast and solutionized material revealed much about their microstructure and composition. Optical microscopy of the as-cast material etched with acetal-picric acid showed extensive coring around zirconium particles and eutectic phase at the grain boundaries (Fig. 2(a)). Using a mean linear intercept method, the average grain size of the as-cast and solutionized material was determined to be 37.5 μm and 81 μm respectively. Figure 2(b) shows the eutectic around the grain boundaries, and some second phase particles inside the as-cast grains. EDS analysis indicated that the intermetallic phase in the eutectic structure is primarily composed of Mg, Nd, Y, and small amounts of other rare earth elements, such as Gd. The SEM image also shows Y-rich cuboids lying around the edges of the eutectic (encircled within the inset in Fig. 2(c)). Figure 3(a) shows the EDS spectrum from one of the Y-rich cuboidal phases observed in the solutionized material.

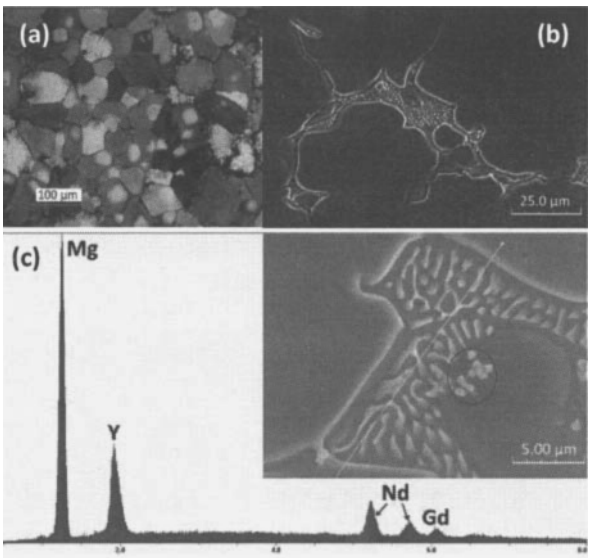

Figure 2. (a) Optical micrograph of contrast etched as-cast WE43. (b) SEM image of the same material, showing grain boundary eutectic and other 2nd phase particles. (c) EDS spectrum of the eutectic phase, showing a Mg-Y-rare earth composition. Y-rich cuboids around the eutectic are circled in the inset image.

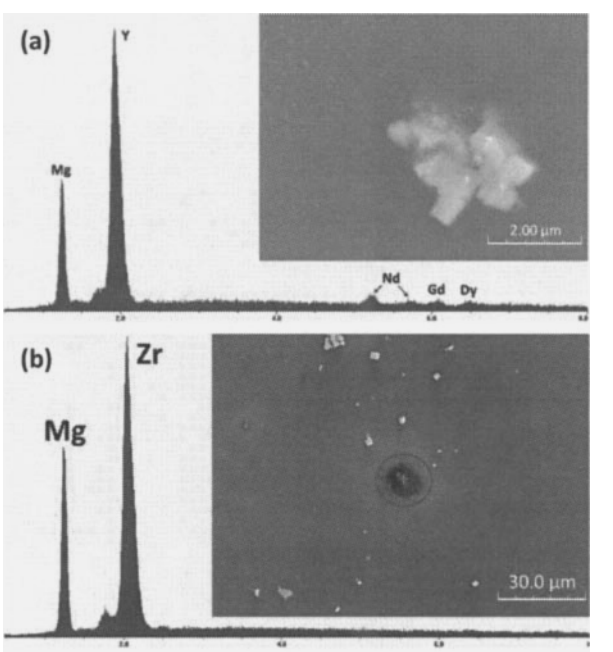

Figure 3. EDS spectra from second phase particles in solutionized WE43 revealed the chemistry of (a) the Y-rich cuboidal precipitates and (b) Zr-rich particles.

In summary, SEM-EDS revealed a eutectic interdendritic region, yttrium-rich cuboidal precipitates around the eutectic, and zirconium-rich particles throughout the as-cast material (Figs. 2 & 3). Only the latter two phases are present in the solutionized material (Fig. 3), i.e. the treatment is effective for dissolution of the eutectic second phase, but not all phases present in the casting. Different homogenization heat treatments will be required if a complete solutionization treatment is desired.

Flow Curves

Effective stress-strain curves obtained at three different temperatures and strain rates are presented in Figure 5, and provide a comparison of the as-cast and solutionized conditions. At the rates examined, the alloy did not exhibit sufficient ductility for hot deformation processing below 350°C, so only those conditions are shown in this first analysis. As there is no reduction in cross-sectional area during torsion testing, the peaks in these torsional flow curves are viewed as evidence of dynamic recrystallization (DRX) [18, 19]. Optical micrographs of deformed samples offered further confirmation of the presence of DRX. The average grain size increased in both the as-cast and solutionized samples. In the solutionized sample shown in Figure 4, new, smaller grains can be observed to have nucleated, mainly at the grain boundaries. The figure also shows evidence of significant precipitation within the grains and along the grain boundaries. These particles may serve to pin the original grain boundaries and impede growth of the new grains which nucleate during DRX. It is concluded that DRX is a pre-requisite for hot workability in this alloy to avoid premature failure by cracking [20].

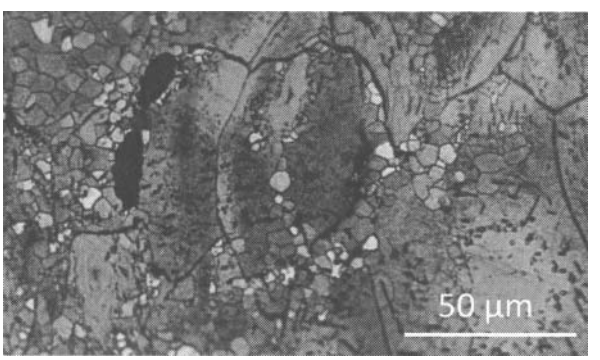

Figure 4. Optical micrograph of a WE43 torsion sample tested at 400°C and 1.0 s^{-1}. The micrograph, taken near the periphery of the sample, shows the presence of dynamic recrystallization.

As seen in Figure 5, the solutionized material was stronger than the as-cast under most conditions. This suggests that having the rare earth elements in solution (and/or dynamically precipitating) is a more effective high temperature strengthener than having the alloy additions bound up in an interdendritic eutectic second phase. The failure of the as-cast samples is thought to be caused by void nucleation at the large, brittle interdendritic second phase particles. The similar behavior of the alloy in the as-cast and solutionized conditions at the higher testing temperatures suggests that the working temperatures may have been sufficiently high that a degree of homogenization occurred during testing in the as-cast material. There was no obvious effect of the larger initial grain size of the solutionized material on the strength or ductility.

Adiabatic heating and Dynamic Strain Aging

Figure 6(a) shows the flow stress at an effective strain of 0.1 plotted as a function of strain rate. This type of graph is used to determine the positive stress exponent of an assumed power law relationship between strain rate and flow stress [10]. However, these data show a different trend. At the lowest temperature and strain rates, there was either rate insensitivity or negative rate sensitivity. At the higher rates (>0.1 s^{-1}), negative rate sensitivity was exhibited at almost all temperatures examined. In the former case, the low rate sensitivity was attributed to dynamic strain aging. In the latter, adiabatic deformation heating was likely the cause.

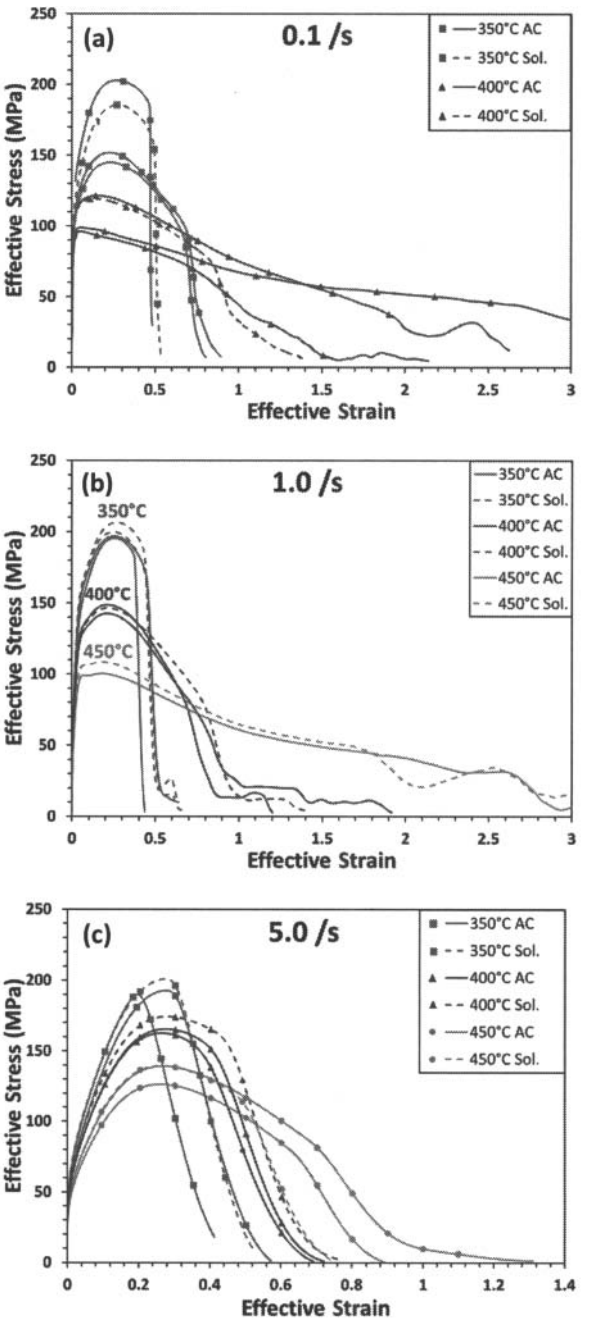

Figure 5. (a- c) Flow curves for as-cast and solutionized WE43 at three different temperatures and strain rates. Multiple curves with the same line style indicate duplicate tests at the same condition.

During torsion testing, work is put into the sample and, under certain conditions, can result in a significant temperature increase [14]. To determine the rate of temperature increase at a strain of 10%, the following equation was used:

$$\dot{T} = (\eta \dot{\varepsilon} \sigma_{0.1})/(\rho c_p) \quad (3)$$

where η is an efficiency factor taken to be 0.95, $\dot{\varepsilon}$ is the nominal strain rate, $\sigma_{0.1}$ is the stress at a strain of 0.1, ρ is the material density taken as 1.84 g/cm^3, and c_p is the specific heat taken to be 0.966 J/kg/K.

While it is admitted that heat transfer can occur radially as well as axially, only heat conduction along the axis and through the grips was considered. Samples were held at temperature for ten minutes prior to testing to minimize any radial temperature gradient. However, the temperature gradient from the sample to the grips that extend out of the furnace into the air may be significant. The dissipation of heat to the grips was calculated using a Fourier series solution to the heat equation:

$$u(x,t) = \sum_{n}^{4} c_n \sin(n\pi x/L)\exp\left(-n^2\pi^2\alpha t/L^2\right) \quad (4)$$

$$c_n = \frac{2}{L}\int_0^L \Pi(\xi)\sin(n\pi\xi/L)d\xi \quad (5)$$

where L is the gage length of the sample, x is the position along the gage length, t is time, and $\alpha = \kappa/(\rho c_p)$, where κ is the thermal conductivity, and ρ and c_p have the same meanings as in Equation 3. $\Pi(\xi)$ is the initial condition of the sample, and was taken to be a Heaviside step function with amplitude equal to the total adiabatic temperature gain calculated from Equation 3. It was determined that at rates of 0.01 s^{-1} and lower, the heat could dissipate faster than it was produced, so the tests can be assumed to be isothermal. At strain rates of 1.0 and 5.0 s^{-1}, the heat is produced in a much shorter time than is required to dissipate any appreciable amount, and thus these tests are assumed to be adiabatic. Tests performed at 0.1 s^{-1} were found to be neither isothermal, nor completely adiabatic. In other words, heat was produced and dissipated at comparable rates. To estimate the temperature rise during these tests, Equations 3 and 4 were integrated incrementally by dividing the time required to reach an effective strain of 0.1 into ten equal steps, and the heat addition and dissipation were estimated for each step.

The data presented in Figure 6(b) has been adjusted to account for this adiabatic heating effect. The rate sensitivities at higher temperatures all appear positive, after making this correction. However, a strength anomaly, where the flow stress remains constant or increases with increasing temperature or decreasing strain rate, still occurs within the lower temperature regime (150-250°C) at which some of the as-cast samples were tested (see left hand side of Fig. 6(b)). This anomaly is associated with dynamic strain aging (DSA) [21, 22, 23, 24]. The final piece of evidence for DSA is presented in Figure 7, a magnified plot of flow curves that clearly exhibit the serrated flow known as the Portevin-Le Châtelier (PLC) effect.

It has been shown that the PLC effect is caused by dynamic strain aging, which is the result of the interaction between solute atoms and dislocations, where the dislocations are repeatedly pinned by solute atmospheres and then able to break away before being pinned again [22, 23, 25]. It is often associated with a loss of uniform ductility [25]. Several different studies of Mg-RE alloys have shown the temperature and strain rate regime for DSA and PLC to be roughly 150-350°C and on the order of 5.5×10^{-5}- 6.0×10^{-3}, respectively [22, 26, 27, 28]. Surprisingly, these alloys do not appear to suffer a loss in ductility. It has been speculated that this is due to the relatively high homologous temperature at which the effect is observed, and the fact that dynamic recrystallization may be occurring simultaneously [21].

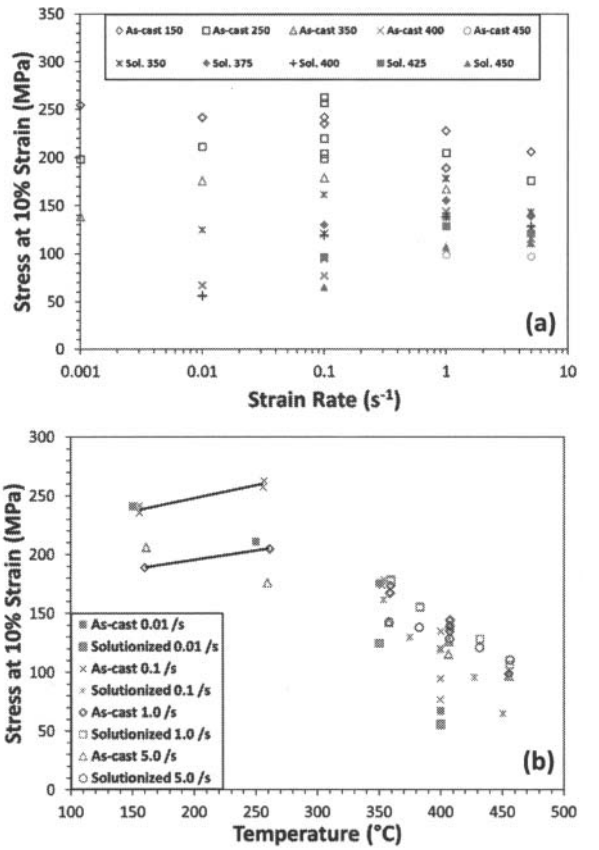

Figure 6. (a) Strain rate vs. flow stress at a strain of 0.1, showing certain regimes of negative strain-rate sensitivity. (b) Temperature vs. flow stress, showing rates that have a positive correlation.

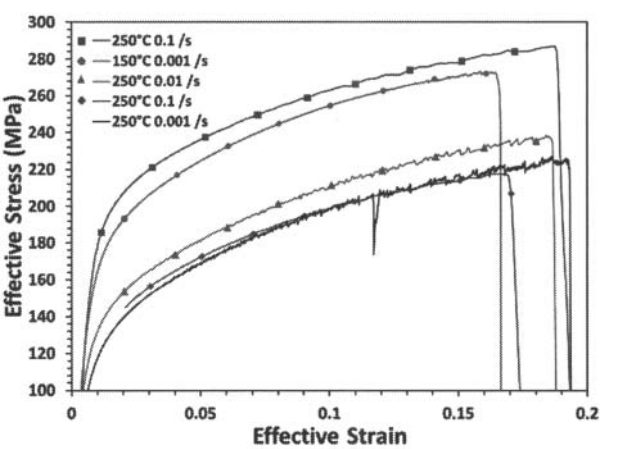

Figure 7. Serrated flow curves showing evidence of the PLC effect in as-cast material.

Constitutive modeling

The temperature-compensated strain rate, or the Zener-Holloman parameter, Z, is defined as,

$$Z = \dot{\varepsilon}\exp(Q/RT) \quad (6)$$

where $\dot{\varepsilon}$ is the strain rate, Q is the activation energy, R is the gas constant, and T is the absolute temperature. Using a single value of Q = 297 kJ/mol, as reported by Gao et al. for similar conditions [15], the low Z data did collapse into a single linear band (Fig. 7). Thus, at low stresses and values of Z, there is a power law relationship between Z and stress (i.e. linear in the log-log plot, Fig. 8).

$$Z = A\sigma^{n^*} \tag{7}$$

where A is a constant, σ is the flow stress, n^* is the stress exponent (or inverse strain rate sensitivity.) In this region, the power law fit, typical of high temperature creep [15, 29], is achieved with values of $A = 10^{8.9}$ and $n^* = 6.8$. These values agree well with those reported in the literature, even those obtained by other modes of deformation, such as tension [30].

It is very convenient that the Zener-Holloman parameter and power law fit work well over the range of temperatures and strain rates relevant to deformation processing at temperatures greater than 350°C. At lower temperatures, the material does not exhibit enough ductility for processing at feasible rates. Furthermore, the alloy exhibits different, sometimes negative, strain rate sensitivities at these lower temperature conditions. While the data from the low temperature tests can be collapsed into the same band in Figure 7 if lower activation energies are used for the 150 and 250°C tests, the fit would still not capture the observed negative strain rate sensitivity. Similarly, the Sellars-Tegart equation, which has successfully described the behavior of other Mg alloys over a wide range of temperatures and strain rates, cannot capture the behavior of low temperature tests for WE43. While the Sellars-Tegart equation permits the stress dependence to become much stronger (i.e., exponential) at high stress levels, typical of power law breakdown [10, 11], it does not have any provision to describe the observed negative strain rate sensitivity.

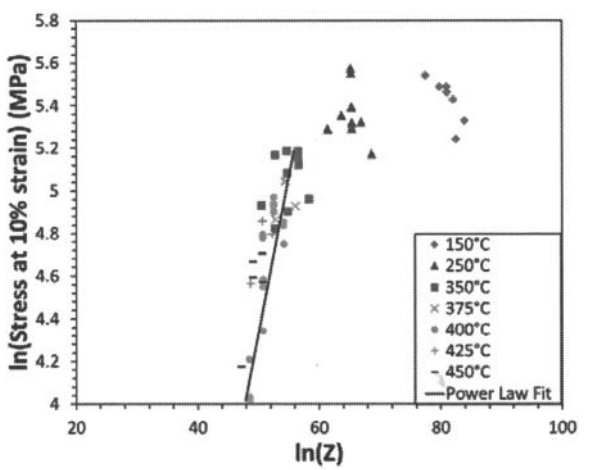

Figure 8. All torsion data with a simple power law fit that reasonably captures the low Z behavior. Data points labeled according to the nominal testing temperature (though the data are adjusted for adiabatic heating.)

Finally, the initial assumption that the strain rate sensitivity, m = 0.132, and strain hardening coefficient, n = 0, are valid for some, but not all test conditions. The strain rate sensitivity (inverse of the stress exponent), n^*, calculated for low Z tests is ~0.147, resulting in negligible error when calculating the flow stress. The assumption that the strain hardening coefficient is zero is only valid at the highest temperature and lowest rate tests. At all other conditions, there is obvious strain hardening occurring, meaning that the value of n needs to be calculated and included in subsequent analyses.

Conclusions

(1) Scanning electron microscopy showed the presence of grain boundary eutectic in the as-cast material, which dissolved during conventional solutionization treatment.

(2) Yttrium-rich cuboidal precipitates and zirconium-rich particles present in the as-cast alloy were not dissolved by the conventional solutionization treatment.

(3) During hot torsion testing, adiabatic heating occurred in magnesium alloy WE43 at high strain rates, namely 1.0 and 5.0 s^{-1}.

(4) If the adiabatic heating is taken into account, the plastic flow of WE43 can be modeled using a simple power law relationship, $n^* \sim 7$, with a single apparent activation energy, $Q \sim 297$ kJ/mol, for the high temperature ($350 \leq T \leq 450$°C) conditions presently examined which appear relevant to deformation processing.

(5) To achieve necessary ductility during processing, deformation must be at a temperature of at least 350°C.

(6) At the lower temperatures, the behavior could not be modeled by the power law or even the more complex hyperbolic sine function of the Sellars-Tegart equation. A model that accounts for dynamic strain aging must be used to capture the behavior of as-cast or solutionized alloy WE43 at low strain rates ($\leq 10^{-1}$ s^{-1}) and low temperatures (150-250°C), where the Portevin-Le Châtelier effect, i.e. serrated flow, was observed.

Acknowledgements

This research was sponsored by the Army Research Laboratory and was accomplished under Cooperative Agreement No. W911NF-07-2-0073. The views and conclusions contained in this document are those of the authors and should not be interpreted as representing the official policies, either expressed or implied, of the Army Research Laboratory or the U.S. Government. The U.S. Government is authorized to reproduce and distribute reprints for Government purposes notwithstanding any copyright notation hereon. The authors would also like to gratefully acknowledge Mr. Pritom Das for performing many of the torsion tests.

References

1. Turski, M., J. F. Grandfield, et al. (2010). "Computer Modeling of DC casting magnesium alloy WE43 rolling slabs." *Magnesium Technology 2010*: 6.

2. Magnesium Elektron Data Sheet 467. http://www.magnesium-elektron.com/data/downloads/DS467WE43.pdf.

3. Ravi Kumar, N.V. et al. "Effect of alloying elements on the ignition resistance of magnesium alloys," *Scripta Materialia*, 49 (2003), 225-231.

4. Riontino, G., M. Massazza, et al. (2008). "A novel thermal treatment on a Mg-4.2Y-2.3Nd-0.6Zr (WE43) alloy." *Materials Science & Engineering A* **494**: 4.

5. Sanchez, C., G. Nussbaum, et al. (1996). "Elevated temperature behaviour of rapidly solidified magnesium alloys containing rare earths." *Materials Science & Engineering A* **A221**: 10.

6. Mengucci, P., G. Barucca, et al. (2008). "Structure evolution of a WE43 Mg alloy submitted to different thermal treatments." *Materials Science & Engineering A* **479**: 8.

7. Pekguleryuz, M. O. and A. A. Kaya (2003). "Creep resistant magnesium alloys for powertrain applications." *Advanced Engineering Materials* **5**(12): 13.

8. Pekguleryuz, M. and M. Celikin (2010). "Creep resistance in magnesium alloys." *International Materials Review* **55**(4): 21.

9. McQueen, H. J. and M. Sauerborn (2005). "Hot workability and extrusion modelling of magnesium alloys." *Z. Metallkd.* **96**: 7.

10. Takuda, H., H. Fujimoto, et al. (1998). "Modelling on flow stress of Mg-Al-Zn alloys at elevated temperatures." *Journal of Materials Processing Technology* **80-81**: 4.

11. Wang, M., S. Wang, et al. (2010). "Dynamic modeling of twin roll casting AZ41 magnesium alloy during hot compression processing." *Transactions of Nonferrous Metals Society of China* **20**: 6.

12. El Mehtedi, M., S. Spigarelli, et al. (2009). "Comparative study of the high-temperature behaviour of Mg-Al and Mg-Zn wrought alloys." *International Journal of Materials Research* **100**(3): 5.

13. Crossland, I. G. and R. B. Jones (1972). "Dislocation creep in magnesium." *Metal Science Journal* **6**: 5.

14. Semiatin, S. L. and J. J. Jonas (2003). Torsion testing to assess bulk workability. *ASM International: Handbook of Workability and Process Design*. G. E. Dieter, H. A. Kuhn and S. L. Semiatin. **14A:** 33.

15. Gao, J., Q. Wang, et al. (2008). "Microstructure and kinetics of hot deformation WE43 magnesium alloy." *Rare Metals* **27**(4): 5.

16. Ball, E. A. and P. B. Prangnell (1994). "Tensile-compressive yield assymmetries in high strength wrough magnesium alloys." *Scripta Metallurgica et Materialia* **31**(2): 6.

17. Jain, A. and S. R. Agnew (2007). "Modeling the temperature dependent effect of twinning on the behavior of magnesium alloy AZ31B sheet." *Materials Science & Engineering A* **462**: 8.

18. Yang, Z., Q. Guo, et al. (2008). "Plastic deformation and dynamic recrystallization behaviors of Mg-5Gd-4Y-0.5Zn-0.5Zr alloy." *Materials Science & Engineering A* **485**: 5.

19. Al-Samman, T. and G. Gottstein (2008). "Dynamic recrystallization during high temperature deformation of magnesium." *Materials Science & Engineering A* **490**: 10.

20. McQueen, H. J. and C. A. C. Imbert (2004). "Dynamic recrystallization: plasticity enhancing structural development." *Journal of Alloys and Compounds* **378**: 9.

21. Stanford, N., I. Sabirov, et al. (2009). "Effect of Al and Gd solutes on the strain rate sensitivity of magnesium alloys." *Metallurgical and Materials Transactions A* **41A**: 10.

22. Trojanova, Z., P. Lukac, et al. (2005). "Dynamic strain ageing during stress relaxation in selected magnesium alloys containing rare earth elements." *Advanced Engineering Materials* **7**(11): 6.

23. Kubin, L. P. and Y. Estrin (1990). "Evolution of dislocation densities and the critical conditions for the Portevin-Le Chatelier effect." *Acta Metallurgica* **38**(5): 12.

24. Kok, S., A. J. Beaudoin, et al. (2002). "A finite element model for the Portevin-Le Chatelier effect based on polycrystal plasticity." *Modelling and Simulation in Materials Science and Engineering* **10**: 19.

25. Lebyodkin, M., Y. Brechet, et al. (1996). "Statistical behavior and strain localization patterns in the Portevin-Le Chatelier effect." *Acta Materialia* **44**(11): 11.

26. Wang, C. Y., X. N. Zhang, et al. (2007). "Serrated flow in cast ZE43 alloy." *Journal of Materials Science* **42**: 3.

27. Wang, Z. F., W. Jia, et al. (2007). "Study on the deformation behavior of Mg-3.6% Er magnesium alloy." *Journal of Rare Earths* **25**: 5.

28. Zhu, S. M. and J. F. Nie (2004). "Serrated flow and tensile properties of a Mg-Y-Nd alloy." *Scripta Materialia* **50**: 5.

29. Polesak III, F. J., C. E. Dreyer, et al. (2009). "Blind study of the effect of processing history on the constitutive behaviour of alloy AZ31B." *Magnesium Technology* **2009**: 6.

30. Wang, J. G., L. M. Hsiung, et al. (2001). "Creep of a heat treated Mg-4Y-3RE alloy." *Materials Science & Engineering A* **315**: 8.